Nonlinear polarization effects in optical fibers: polarization attraction and modulation instability [Invited]

G. Millot[1,3] and S. Wabnitz[2,4]

[1]*Laboratoire Interdisciplinaire Carnot de Bourgogne (ICB), UMR 6303 CNRS/Université de Bourgogne, Dijon, France*
[2]*Dipartimento di Ingegneria dell'Informazione, Università di Brescia, Via Branze 38, 25123 Brescia, Italy*
[3]*e-mail: Guy.Millot@u-bourgogne.fr*
[4]*e-mail: stefan.wabnitz@unibs.it*

Received July 4, 2014; accepted August 26, 2014;
posted September 15, 2014 (Doc. ID 216335); published October 17, 2014

We review polarization stabilization techniques based on the polarization attraction effect in low-birefringence fibers. Polarization attraction or pulling may be based on cross-polarization modulation, on parametric amplification, and on Raman or Brillouin scattering. We also review methods for laser frequency conversion based on polarization modulation instabilities in low- and high-birefringence fibers, and photonic crystal fibers. Polarization instabilities in nonlinear fibers may also be exploited for sensing applications.

OCIS codes: (060.0060) Fiber optics and optical communications; (060.4370) Nonlinear optics, fibers; (190.4380) Nonlinear optics, four-wave mixing; (230.4320) Nonlinear optical devices; (250.4745) Optical processing devices.
http://dx.doi.org/10.1364/JOSAB.31.002754

1. INTRODUCTION

The state of polarization (SOP) is one of the three physical properties of an electromagnetic wave packet, besides its number of photons and its frequency. Although the management and measurement of the wave energy and frequency have progressed to unprecedented levels of precision, light SOP still remains largely elusive to control in fiber optics communication systems. Indeed, despite the significant progress in optical fiber manufacturing, because of residual birefringence or strain the SOP of a light wave remains virtually unpredictable after propagating over a few hundred meters in a fiber. In recent years, it has been shown that the nonlinearity of low-birefringence optical fibers may be exploited in order to achieve all-optical control and stabilization of the output SOP of a signal beam. This effect is known as polarization attraction or polarization pulling: the signal SOP stabilized though its nonlinear interaction with a CW polarized pump beam.

Combining the polarization degree of freedom with nonlinearity may also lead to polarization instabilities in optical fibers. In the presence of chromatic dispersion, polarization modulation instabilities in optical fibers may be usefully exploited for shifting the frequency of a pump laser to new wavelength regions, and for the generation of ultrashort bright or dark pulse trains.

Because of the extraordinary range of physical phenomena resulting from combining the polarization of light with the nonlinear Kerr effect of optical fibers, it is not possible here to provide an exhaustive review. Therefore, we have chosen to dedicate this mini-review to the discussion of recent progress on polarization stabilization techniques based on the polarization attraction effect in low-birefringence fibers. Moreover, we shall review methods to achieve wideband frequency conversion based on polarization modulation instabilities in birefringent fibers.

2. POLARIZATION ATTRACTION

The development of future transparent all-optical networks demands the availability of devices for the ultrafast all-optical SOP control, which may be enabled by exploiting the nonlinear response of optical fibers. Depending upon the presence of gain for the signal beam whose SOP is to be controlled, there are two basic mechanisms for achieving nonlinear polarization control: (i) dissipative polarizers based on polarization-dependent gain (PDG) and (ii) lossless polarizers exploiting cross-polarization modulation. Devices belonging to the first class are Brillouin, Raman, and parametric amplifiers. These devices do not conserve the energy of the beam and, more importantly, because they are based on polarization selective gain, they suffer from a large amount of output relative intensity noise (RIN). In fact, since only the input signal polarization component which is parallel to the pump gets amplified, SOP fluctuations of the input signal necessarily translate into large output intensity fluctuations. On the other hand, lossless polarizers are RIN-free. Lossless polarizers come in two varieties: in the first type of polarizers, signal SOP control is imposed by means of the cross-polarization interaction with a second pump beam. This interaction can occur either in a counterpropagation or in a copropagation geometry. Counterpropagation leads to full signal repolarization but with the drawback of a response time of the order of the propagation delay across the fiber length, whereas copropagation induces

partial repolarization only; however, since it exploits a traveling wave geometry, it has the advantage of virtually instantaneous operation. In the second type of lossless polarizers, signal polarization control is determined by the self-polarization interaction with its back-reflected replica from a feedback mirror. In addition, more complex functionalities such as digital polarization beam-splitting are permitted by lossless polarizers based on the self-polarization interaction mechanism.

A. Lossless Polarizers

Let us consider first the most intriguing and potentially useful type of nonlinear fiber polarizers, namely lossless polarizers based on the conservative cross- and self-polarization effect. The first class of conservative polarizers involves the injection of a counterpropagating CW pump with a well-defined SOP. The operating principle of the all-optical SOP regeneration in fibers is the following. In the presence of an intense counterpropagating pump beam and for sufficiently high-power signal powers and/or long fiber spans, all input signal SOPs are attracted toward a well-defined SOP at the fiber output. This attracting SOP thus acts as a sort of "polarization funnel," as first described by Heebner *et al.* for a slow photorefractive material [1] and by Pitois and Haelterman for a fast cubic nonlinear fiber [2]. The resulting strength of signal repolarization is largely independent of its input SOP: quite remarkably, the operation of the nonlinear lossless polarizer is not accompanied by any loss of signal power. This is in marked contrast with the case of a linear polarizer: for an input depolarized beam, on average 50% of the power is lost at the polarizer output. Moreover, in a lossless polarizer the input signal SOP fluctuations are not converted into output intensity fluctuations.

B. Theory of Lossless Polarizers

It has been known for a long time that the cross-interaction among intense counterpropagating beams in a Kerr or cubic nonlinear dielectric leads to a mutual rotation of their SOP [3]. Kaplan and Law [4] found exact analytical solutions which exhibit polarization bistability and multistability, as experimentally confirmed by Gauthier *et al.* [5]. The same process is also responsible for leading to both spatial (or longitudinal) [6–10] as well as temporal [11] polarization instabilities and chaos. The general spatiotemporal stability of the nonlinear polarization eigenarrangements (or eigenpolarizations) which remain unchanged upon propagation in a nonlinear anisotropic Kerr medium was analyzed by Zakharov and Mikhailov [12], who pointed out the formal analogy between the equations describing the Stokes vectors associated with the SOP of the two beams and the equations describing the coupling of spin waves in ferromagnetic materials or the Landau–Lifshitz model. The spatiotemporal stability of the eigenpolarizations was later extended to the case of an optical fiber with linear anisotropy, i.e., with elliptical linear birefringence; consider for example a birefringent fiber which is twisted at uniform rate [13]. That study predicted that, for a particular value of the ellipticity of the linear fiber eigenmodes (or the twist rate), the polarization evolution equations for the counterpropagating beams reduce to the chiral model of field theory, which is completely integrable by means of the inverse scattering transform, and exhibits polarization soliton solutions [14–16].

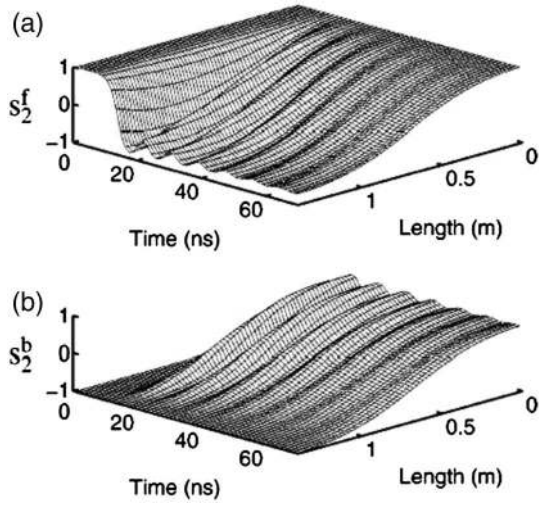

Fig. 1. Simulation of PDW generation with counter-rotating circularly polarized CW beams. $S_2^{(f,b)}$ denotes the dimensionless Stokes parameter associated with the right or left circular polarization component of the forward or backward beam, respectively (from [18]).

In the presence of boundary conditions that fix the SOP of the two beams at opposite ends of the fiber, it was first numerically predicted [17] and later experimentally observed [18,19] the generation of stable domains of mutual stable SOP arrangements, separated by regions of polarization switching or polarization domain wall (PDW) solitons. See for example the simulation result of Fig. 1. Here we inject two counter-rotating circularly polarized waves at opposite ends of the fiber. As can be seen, after an initial transient stage due to propagation delay in the fiber, the SOP of both beams switches to the orthogonal circular polarization as if it was *attracted* to the SOP of the other beam. Indeed, an absolute minimum of the interaction Hamiltonian is reached for counterpropagating waves which maintain the same circular SOP along the fiber. For counterpropagating beams of equal intensities, PDW solitons represent standing waves which remain frozen inside the fiber, much like gap solitons in fiber Bragg gratings [20]. However, for intensity-unbalanced beams, the PDWs slowly move in the forward or in the backward direction, thus enabling the readout of polarization domains that were previously written inside the fiber. This makes PDW solitons potentially useful for all-optical data storage applications [12,15].

Whenever a temporal polarization switching is imposed on a pump beam at one end of the fiber, a polarization switching is also observed in the output signal wave in order to maintain the stable domain arrangement inside the fiber, as experimentally demonstrated by Pitois *et al.* [18,19]. Quite remarkably, the presence of boundary conditions in a fiber of finite length may spoil the temporal stability of the PDW solitons, and lead to different branches of stable polarization attractors, as it was numerically demonstrated in the specific case of a spun elliptically birefringent optical fiber [21,22].

In general, nonlinear polarization interaction among counterpropagating waves may lead to the effective attraction of the output signal SOP toward a particular value which is determined by the SOP of the pump. The first proof-of-principle demonstrations of the polarization attraction effect were obtained using counterpropagating nanosecond pump pulses

and a short span of linearly isotropic highly nonlinear fiber [23–25]. A key breakthrough advance for the practical usage of nonlinear lossless polarizers in telecom applications consisted in the demonstration of 10 Gbit/s on–off-keying (OOK) signal repolarization induced by a sub-Watt CW pump in a few km long span of telecom nonzero-dispersion-shifted fiber (NZDSF) [26,27]. The relevance of this result, which was largely unexpected, stems from the fact that it demonstrates the robustness of nonlinear polarization attraction even in the presence of a locally much stronger linear anisotropy or birefringence, which varies randomly along the fiber.

In fact, as theoretically demonstrated by Kozlov *et al.* [28,29], in the presence of rapidly varying (with respect to the nonlinear interaction length) random linear birefringence, one may obtain averaged propagation equations which describe the nonlinear cross-polarization interaction among the signal and the counterpropagating pump with a good level of accuracy. The availability of a relatively simple deterministic model for describing nonlinear lossless polarizers based on randomly birefringent telecom fibers provides a key tool for numerically estimating their performance. Moreover, the properties of steady-state solutions of the averaged polarization evolution equations may be described in terms of mathematical techniques developed for the study of Hamiltonian singularities [30]. Such approach has led to the interesting observation that polarization attraction is closely linked with the existence of singular tori or multidimensional separatrix solutions [31–33]. A rigorous analytical mathematical proof of the process of temporal relaxation of the signal wave SOP toward a single attracting SOP is not yet available, mostly because of the complication imposed by the boundary conditions in a fiber of finite length. However, a simple understanding of the physical origin of polarization attraction may be given by proving that this effect is associated with the presence of spatiotemporally stable stationary solutions, whereas all other stationary solutions are unstable, so that their decay toward the stable or attracting polarization arrangements occurs in the experiments [34].

Consider the conservative polarization interaction between intense signal and counterpropagating pump beams in a randomly birefringent telecom optical fiber span. The dimensionless evolution equations for Stokes vector of the forward signal beam, $\vec{S}^+ = (S_1^+, S_2^+, S_3^+)$, and of the backward pump beam, $\vec{S}^- = (S_1^-, S_2^-, S_3^-)$, read as [28,29]

$$\begin{aligned}(\partial_t + \partial_z)\vec{S}^+ &= \vec{S}^+ \times \hat{J}_\times \vec{S}^-,\\ (\partial_t - \partial_z)\vec{S}^- &= \vec{S}^- \times \hat{J}_\times \vec{S}^+,\end{aligned} \tag{1}$$

where z is distance, t is time, $\times$ denotes the vector cross product, and the cross-polarization tensor is defined as $\hat{J}_\times = \mathrm{diag}(-1, 1, -1)$. No fiber loss has been taken into account because of the relatively short lengths (up to 10 km) of fiber involved in devices based on the polarization attraction effect. In this case, the beam powers are conserved quantities. The average Eqs. (1) are justified in the so-called Manakov limit [35], namely, whenever both the nonlinear length $L_{\mathrm{NL}} \equiv 1/\lambda S_0^+$ (here γ is the nonlinear Kerr coefficient and S_0^+ is the power of the forward signal beam) and the total fiber length L are much shorter than the polarization mode dispersion (PMD) diffusion length $L_D \equiv 3/D_p^2(\omega_+ - \omega_-)^2$, where D_p is the PMD coefficient and $\omega_\pm$ are the angular frequencies of the two beams [36,37]. Cross-polarization interactions in different types of fibers (e.g., perfectly isotropic, high-birefringence, or spun fibers) are described by equations similar to Eqs. (1) but including an additional self-polarization rotation term.

Equations (1) can be conveniently reduced to a symmetric form by using the new Stokes vector definitions $\vec{S} = \vec{S}^+$ and $\vec{H} = -\hat{J}_\times \vec{S}^-$, so that

$$\begin{aligned}(\partial_t + \partial_z)\vec{S} &= \vec{H} \times \vec{S},\\ (\partial_t - \partial_z)\vec{H} &= \vec{H} \times \vec{S},\end{aligned} \tag{2}$$

hold, in addition with the boundary conditions $\vec{S}(0) = \vec{S}_0$ and $\vec{H}(L) = \vec{H}_L$. In the steady-state, i.e., whenever $\partial_t \vec{S} = \partial_t \vec{H} = 0$, Eqs. (2) have the exact analytic solution

$$\mu = F(\eta) = \frac{(H\eta + S)(H + S\eta)}{H^2 + S^2 + 2HS\eta}(1 - \cos \Omega L) + \eta \cos \Omega L, \tag{3}$$

where

$$\eta = \frac{(\vec{H}_L \cdot \vec{S}_L)}{HS}, \qquad \mu = \frac{(\vec{H}_L \cdot \vec{S}_0)}{HS}, \tag{4}$$

represent the alignment factor between the input pump at $z = L$, and the signal at either the output $z = L$ or the input $z = 0$ end of the fiber, respectively; moreover, $\vec{\Omega} = \vec{H} + \vec{S}$, $H^2 = \vec{H} \cdot \vec{H}$, and $S^2 = \vec{S} \cdot \vec{S}$, which remain invariant along the fiber, i.e., $\partial_z \vec{\Omega} = \partial_z S = \partial_z H = 0$. By inverting Eq. (3), one may obtain the pump-signal polarization alignment at the fiber output η as a function of their alignment at the respective fiber input, or μ.

Figure 2(a) provides a graphical illustration of the solution of Eq. (3) for equal signal and pump intensities. As can be seen, for a given μ there are in general multiple branches of solutions for the output polarization alignment η. However, the numerical stability analysis of the stationary solution of Eq. (3) shows that only the lowest branch, corresponding to the lowest value of the output SOP alignment η, is temporally stable [34]. As can be seen in Fig. 2(a), for relatively large beam powers or fiber lengths, in the lowest branch of the solution of Eq. (3) one obtains an antiparallel output alignment $\eta \cong -1$ for any input signal-pump alignment μ, namely, for any signal SOP value at the fiber input. In other words, irrespective of its initial value, the SOP of the signal is attracted toward an output SOP which is orthogonal to the polarization of the input counterpropagating pump. This property is visualized in Fig. 2(b), where we show the dependence of the averaged (over the input signal SOP) output polarization alignment of the signal, as a function of its power. Figure 2(b) also shows that, for obtaining efficient polarization attraction, the powers of the signal and pump should be matched. In fact, the overall picture of the domain of polarization attraction as a function of pump and signal powers is given in Fig. 2(c). As can be seen, for relatively small powers of either the pump or the signal, there is only one stable branch of stationary solutions of Eq. (3) and no global polarization attraction is observed (white region). Conversely, for high signal and pump powers (shaded region) there is a stable branch of solutions of Eq. (3) which leads to polarization attraction. However, this

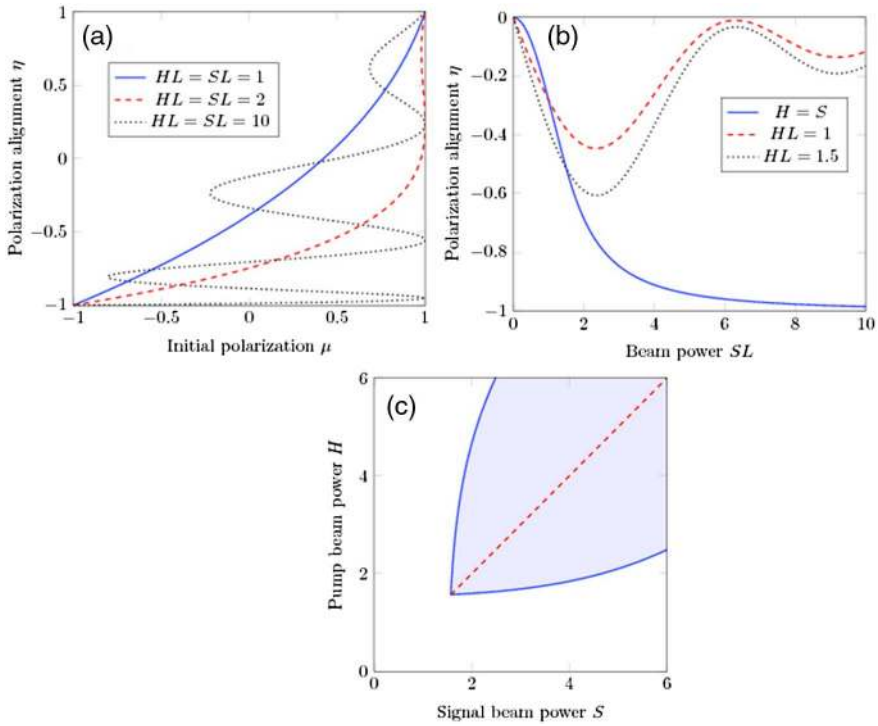

Fig. 2. (a) Relation between output η and input μ polarization alignment parameters. (b) Output signal-pump average polarization alignment parameter versus signal beam power, for different values of pump power. (c) Diagram of different polarization attraction regimes (reprinted from [34] with permission from Elsevier).

polarization attraction is not global (i.e., it does not cover the entire Poincaré sphere for the signal SOP), unless $H = S$ and H, $S > \pi/2L$, in which case the analysis of the algebraic curves defined by Eq. (3) shows that polarization attraction is obtained for all values of the initial alignment $-1 \le \mu \le 1$ (dashed red line). Although the previously described analytical approach provides valuable insight into the physical mechanism for polarization attraction, for practical purposes the optimization of the design and estimation of the performance of a lossless polarizer requires extensive numerical computations [38].

C. Experiments with Lossless Polarizers

Let us describe now two examples of experimental studies of nonlinear lossless polarizers, which demonstrated the regeneration of the SOP of 40 Gbit/s OOK return-to-zero (RZ) signals. The initial setups involved an independent CW counterpropagating pump [39,40]. The polarization-scrambled input signal was injected into a low-PMD fiber with normal group velocity dispersion (GVD). The 40 Gbit/s RZ signal was generated by means of a 10 GHz mode-locked fiber laser delivering 2.5 ps pulses at 1564 nm. A programmable liquid-crystal-based optical filter was permitted to temporally spread the initial pulses so as to obtain 7.5 ps Gaussian pulses by spectral slicing. The resulting pulse train was intensity modulated by a $LiNbO_3$ modulator through a $2^{31} - 1$ pseudo-random bit sequence. A 2-stage bit-rate multiplier was used to generate the 40 Gbit/s RZ bit signal stream. Large and fast fluctuations of the signal SOP were induced via a polarization scrambler operating at 650 Hz. Before injection into the fiber, the 40 Gbit/s signal was amplified by means of an erbium-doped fiber amplifier to the average power of 27 dBm. The fiber used for demonstrating the polarization attraction effect was a 6.2 km long nonzero dispersion-shifted fiber (NZDSF) with chromatic dispersion $D = -1.5$ ps/nm/km at 1550 nm, nonlinear parameter $\gamma = 1.7\ \mathrm{W^{-1}\,km^{-1}}$, and PMD coefficient $D_p = 0.05\ \mathrm{ps/km^{1/2}}$. Two optical circulators were inserted at both fiber ends, so as to inject and collect both waves.

The external pump was provided by a 1 W continuous incoherent wave with fixed but arbitrary SOP, the spectral linewidth of 100 GHz and the central wavelength of 1545 nm. At the receiver, a polarizer was inserted for translating SOP fluctuations into intensity fluctuations. Behind the polarizer, the 40 Gbit/s eye diagram was monitored by means of an optical sampling oscilloscope, and the signal SOP was also recorded onto the Poincaré sphere using a polarimeter.

The efficiency of polarization attraction was experimentally measured by evaluating the output signal degree of polarization (DOP) as a function of pump power. The DOP is defined as $\mathrm{DOP} = \sqrt{\langle S_1^+\rangle^2 + \langle S_2^+\rangle^2 + \langle S_3^+\rangle^2}$, where $\langle\rangle$ denotes averaging over 256 randomly chosen input polarizations. As can be seen in Fig. 3, the DOP of the signal wave, which has initially a low level due to its initial scrambling, increases and reaches

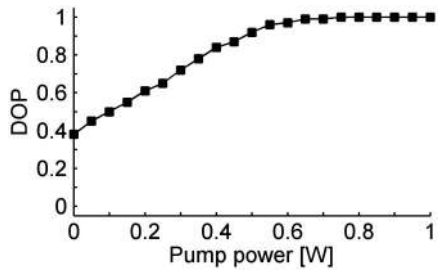

Fig. 3. Experimental DOP as a function of pump power (from [40]).

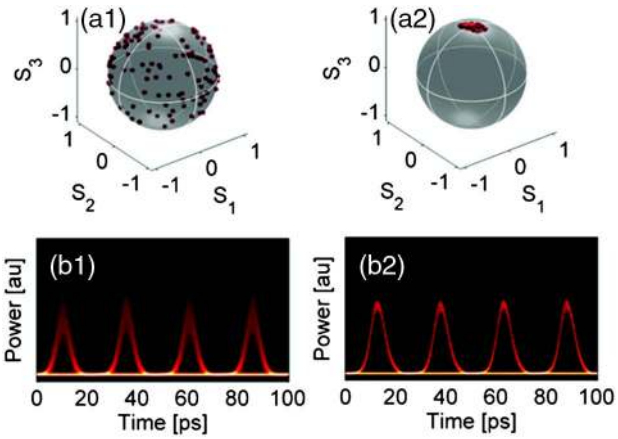

Fig. 4. (a) Output SOP and (b) eye diagram behind a polarizer of the 40 Gbit/s signal with input SOP polarization scrambling (1) without and (2) with the counterpropagating pump wave (from [40]).

unity as the pump power grows above 500 mW. Note that this threshold pump power corresponds to the condition of equal average signal and pump powers.

The performances of polarization attraction were quantified in real-time by means of the SOP monitoring and eye diagram visualization (see Fig. 4). Without the pump beam, because of the initial polarization scrambling process, the signal SOP is uniformly spread onto the whole Poincaré sphere [Fig. 4(a1)], so that the eye diagram behind the polarizer is completely closed [Fig. 4(b1)]. On the other hand, in the presence of the pump beam all output signal SOPs collapse to a small spot on the Poincaré sphere [Fig. 4(b1)]. The corresponding output eye diagram of Fig. 4(b2) is fully open, thus confirming highly efficient polarization attraction.

When a separate pump beam is used, the output signal SOP depends on the input pump SOP. Let us now consider replacing the pump with an output reflective element composed of a fiber coupler (90/10), a polarization controller, and an EDFA [40,41]. The corresponding reflection coefficient R is defined as the ratio between the powers of reflected and input signals: thanks to the active control loop, R can be lower than, equal to, or larger than one. Quite remarkably, with the adjustable mirror the output signal SOP remains circularly polarized, irrespective of the SOP of the back-reflected wave. Figure 5

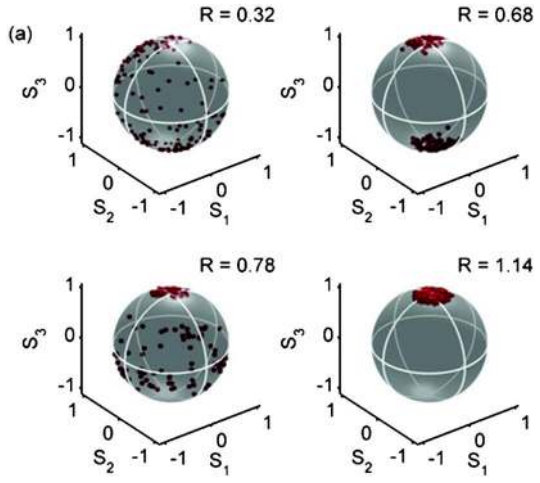

Fig. 5. (a) Evolution of the signal SOP at the reflective polarizer output for different values of the reflection coefficient R (from [40]).

shows the evolution on the Poincaré sphere of the signal SOP at the fiber output for different values of R. As can be seen, for $R = 0.32$ all SOPs in the north (south) hemisphere, corresponding to right (left) SOPs, are partially attracted toward the corresponding pole. Whenever $R = 0.68$, the output SOPs remain confined in two small spots around the two poles (i.e., the right- or left-handed circular polarizations): the fiber operates as a digital beam splitter for the SOP of light. As R is increased up to $R = 0.78$, the domain of attraction which was previously located around the south pole loses stability, and all of the output signal SOPs get attracted by the north pole. Global (i.e., with equal strength irrespective of the input SOP) polarization attraction is reached for $R = 1.14$: all the SOPs of the output signal wave remain localized within a small surface around the north pole. Note that full convergence around the south pole could also be observed, depending on the setting of a polarization controller which is inserted into the reflective loop.

From the practical viewpoint, an important parameter is the maximum operating speed of a nonlinear lossless polarizer. In fact, theory and experiments agree well in evaluating the signal propagation delay through the fiber span as a typical estimate of the response time of the nonlinear polarizer [42]. As a result, polarization tracking speeds of 200 krad/s could be reached when using a 6 km long NZDSF [43]. Nonlinear SOP regenerators may have their operating power levels or associated fiber length much reduced, by using highly nonlinear and birefringent or spun optical fibers [44,45].

Since polarization attraction is based on the virtually instantaneous Kerr response mechanism of silica fibers, ultrafast signal polarization control may be achieved by exploiting the nonlinear cross-polarization interaction with a copropagating CW pump at a different carrier frequency. However, in the copropagating regime the efficiency of polarization attraction is much reduced when using CW beams: the peak signal DOP is equal to 0.73 and its asymptotic value is as low as 0.5 [46]. Nevertheless, signal DOPs above 0.8 can be obtained even in the copropagating pump configuration by cascading multiple lossless polarizers. Moreover, in the practical relevant case of short signal pulses, the output DOP may be substantially increased by properly increasing the temporal walk-off between the signal pulses and the CW pump. In fact, in the presence of group-velocity-induced walk-off, the signal meets fresh portions of the original polarized CW pump as it propagates; hence, the efficiency of repolarization is increased [47].

Lossless polarization attraction in high-birefringence fiber has been recently experimentally studied: in this case, one may obtain attraction toward a specific line of SOPs on the surface of the Poincaré sphere, instead of a particular polarization state [48]. This shows that the properties of polarization attraction strongly depend on the linear and nonlinear anisotropy properties of the optical fiber. Moreover, based on the polarization bistability shown in Fig. 2(a), it was possible to demonstrate the application of lossless polarization attraction to implement an all-optical flip-flop memory and data packet switching operation [49].

D. Dissipative Polarizers

As it is well-known, stimulated Brillouin, Raman, and parametric amplifications in optical fibers are strongly polarization

dependent. In fact, in all of these cases, virtually the polarization component of the signal which is parallel to the pump beam only experiences gain, whereas the orthogonal component is not amplified. In optical fibers, the situation is more complicated because of the presence of linear birefringence. As in all stimulated scattering processes the pump and the signal beams have different wavelengths, and because of the wavelength dependence of linear birefringence, after a certain distance the SOP of the signal is decorrelated with respect to the SOP of the pump. As a result, whenever the amplification distance is longer than the PMD diffusion length L_D, the pump SOP is effectively scrambled by fiber birefringence. Therefore, in this limit case, which we define as the diffusion regime, the signal experiences a depolarized or polarization-averaged gain which is simply half of the maximum gain that is obtained for parallel pump and signal SOPs [50].

The situation is drastically different when an ultralow PMD fiber is used for signal amplification by using either parametric or stimulated scattering in the presence of high-power pump waves. In this case, the nonlinear length may be smaller than the diffusion length L_D. Therefore, the signal is amplified well before birefringence-induced decorrelation among the signal and the pump SOPs may take place. As a result, because of the polarization-selective gain, in this limit (which, as it was the case for lossless polarizers, is also defined as the Manakov limit) the signal SOP is effectively pulled (or attracted) toward the pump SOP.

Polarization attraction using a Raman gain-activated polarizer was numerically studied [51,52] and experimentally validated in Ref. [51]. In that work, its authors have shown that initially unpolarized light is amplified and, as the copropagating pump power grows larger, is simultaneously repolarized after propagation in a low-PMD, randomly birefringent dispersion-shifted fiber. Namely, the SOP of the signal beam at the output of the fiber is attracted toward the SOP of the outcoming pump beam (see Fig. 6). Stimulated by this result,

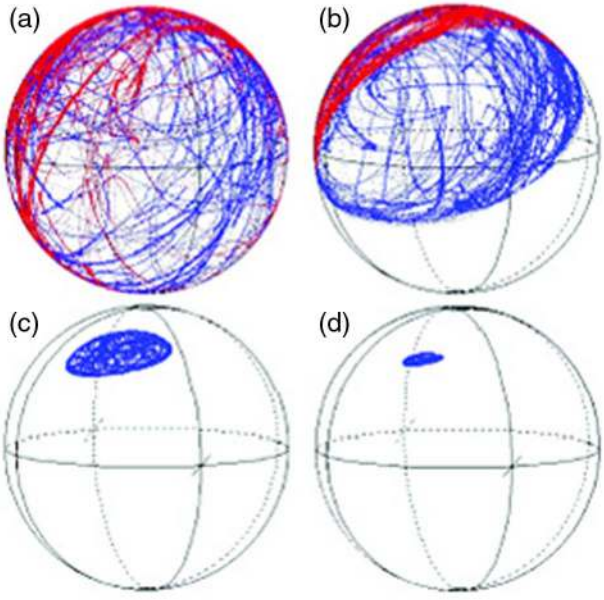

Fig. 6. Output signal SOP from a copropagating Raman polarizer, visualized on the Poincaré sphere for a scrambled input SOP. The input polarized pump power was (a) 0.6 W, (b) 0.75 W, (c) 1.3 W, and (d) 2.2 W (from [51]).

theoretical descriptions of the operation of Raman polarizers in both copropagating and counterpropagating configurations were subsequently developed [53,54]. Moreover, the possibility of suppressing the output signal RIN by operating in the pump saturation regime was proposed [55], and the possible application of a Raman polarizer to the simultaneous amplification and repolarization of multiple wavelength channels was also numerically demonstrated [56].

Quite remarkably, in either the diffusion or the Manakov limit situation the operation of a Raman polarizer may be described by means of a simple and analytically tractable model. In the diffusion limit the polarizer acts as a standard, depolarized Raman amplifier, whereas in the Manakov limit the Raman polarizer behaves as an ideal polarizer, leading to the complete alignment of the output signal SOP with the pump SOP [57].

Let us consider the propagation of signal and pump beams in a few kilometers long span of low-PMD, randomly birefringent telecom fiber. A detailed vectorial theory of Raman amplification in randomly birefringent or spun optical fibers was developed by Lin and Agrawal [58] and Sergeyev *et al.* [59], respectively, for describing the operation of depolarized standard Raman amplifiers (i.e., in the diffusion limit). Namely, these studies analyzed the statistics of PMD-induced fluctuations of the intensity of the amplified signal. On the other hand, in the Manakov limit the evolution of the Stokes vector of the signal $\vec{S}^s$ obeys

$$\partial_z \vec{S}^s = \vec{S}^s \times \hat{J}_\times \vec{S}^p + \frac{g}{2}[S_0^p \vec{S}^s + S_0^s \hat{J}_R \vec{S}^p], \tag{5}$$

where $\vec{S}^p$ is the Stokes vector of the pump beam, and g is the ratio of Raman gain and Kerr coefficients of the fiber. Moreover, the cross-polarization rotation tensor $\hat{J}_\times = \mathrm{diag}(-1,-1,-1)$ and the Raman tensor $\hat{J}_R = \mathrm{diag}(1,1,1)$ for a copropagating pump, whereas $\hat{J}_\times = \mathrm{diag}(-1,1,-1)$ and $\hat{J}_R = (1/3)\mathrm{diag}(1,-1,1)$ for a counterpropagating pump, respectively. In both cases, Eq. (5) may be analytically solved. By defining the average (over the ensemble of input signal SOPs which are supposed to be equally distributed on the Poincaré sphere) output gain as $G \equiv \langle S_0^s(z=L)\rangle / \langle S_0^s(z=0)\rangle$, one obtains for G and the DOP in the codirectional geometry

$$G = \frac{1+\exp(gPL)}{2}, \qquad \mathrm{DOP} = 1 - \frac{1}{G}. \tag{6}$$

On the other hand, in the counterdirectional case one has

$$G = \frac{\exp(2gPL/3) + \exp(gPL/3)}{2}, \qquad \mathrm{DOP} = 1 - \sqrt{\frac{2}{G}}. \tag{7}$$

Moreover, in both cases simple analytical expressions can also be found for the PDG (i.e., the difference between maximum and minimum gain), as well as for the RIN variance [57]. By comparing Eqs. (6) and (7), it turns out that the average signal gain is larger in the copropagating geometry, but in both cases the gain is larger than in the case of a standard Raman amplifier operating in the diffusion limit, where $G \propto \exp(gPL/2)$. On the other hand, the counterpropagating ideal Raman polarizer has the advantage that the signal SOP is attracted toward the fixed input pump SOP at $z = L$, whereas in the copropagating geometry the signal is attracted

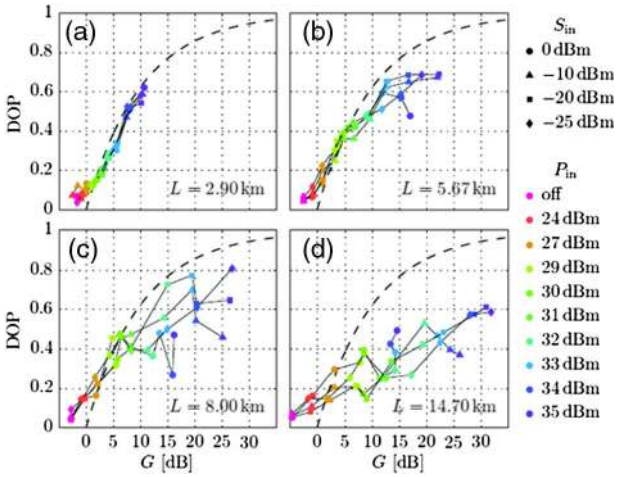

Fig. 7. Measured signal DOP for a counterpropagating Raman polarizer as a function of the gain G for different pump (P_{in}) and signal (S_{in}) input powers, and for four different fiber lengths L. Dashed curves represent Eq. (7) (from [60]).

toward a generally unknown output pump SOP at $z = L$, which moreover is subject to environmental fluctuations of the linear birefringence of the fiber.

A detailed experimental verification of polarization attraction in a Raman polarizer operating in the counterpropagating geometry was performed by Chiarello *et al.* [60]: the validity of Eq. (7) was confirmed for relatively short lengths of NZDSF (see Fig. 7). For fiber lengths larger than about 6 km, the repolarization is reduced because of gain saturation, as well as the PMD-induced polarization decorrelation between the pump and signal [61].

As we have seen, Raman polarizers are also very efficient Raman amplifiers (with a doubled gain coefficient in the codirectional geometry). However, they suffer from large PDG because all input SOP fluctuations are amplified into large intensity fluctuations; hence, the resulting high RIN severely limits their potential application. In order to achieve efficient signal SOP pulling with much reduced PDG, it has been proposed by Sergeyev to use a two-stage approach by using a cascade of two fibers [62–64]. The first fiber has a fast spinning of the local birefringence axes, so that the SOP of the pump and signal is fully decorrelated at its output, for any value of the input signal SOP. The second fiber exhibits a slow spinning of the fiber axes, thus acting as a classical Raman polarizer which pulls the signal SOP toward the pump SOP. The polarization decorrelation introduced by the first fiber leads to much reduced input SOP fluctuations (hence, output RIN) for the subsequent Raman polarizer.

Similar to Raman-based polarizers, dissipative polarizers may also be based on stimulated Brillouin scattering. In fact, pulling of the signal polarization toward the pump SOP has been theoretically analyzed and experimentally demonstrated in Brillouin amplifiers [65–67].

Besides stimulated Raman and Brillouin scattering, polarization attraction may also occur in parametric four-photon scattering processes in optical fibers. For example, it has been theoretically predicted that FWM in a highly birefringent optical fiber in the presence of a dual-polarization pump wave may lead to polarization attraction for the Stokes and anti-Stokes waves both in the normal and in the anomalous dispersion regime [68]. The impact of random birefringence on vector FWM processes in optical fibers was studied by Lin and Agrawal [69,70] and McKinstrie *et al.* [71]. In the anomalous dispersion regime, parametric amplification or induced modulation instability in a low-PMD fiber operating in the Manakov limit leads to polarization attraction of both the signal and the generated idler toward the same SOP of the pump [72]. The averaged equations describing three-wave mixing in a parametric polarizer based on a randomly birefringent telecom fiber were derived in Ref. [73], and efficient polarization attraction was experimentally demonstrated by using a low-PMD highly nonlinear fiber by Stiller *et al.* [74].

Since parametric and Raman scattering are simultaneously present in optical fibers [75], they can be exploited in combination with polarization cross-modulation in order to achieve efficient polarization attraction. Moreover, it has been theoretically demonstrated that polarization pulling in a low-PMD Raman amplifier is broadband: its bandwidth extends over about 60 nm around the Raman peak Stokes shift of 13.2 THz [76]. As a result, broadband polarization attraction resulting from the combination of Raman amplification and cross-phase modulation was experimentally observed both in a few meters of isotropic fiber [23], as well as in a few km long randomly birefringent telecom fiber [77].

3. CROSS-POLARIZATION MODULATION-INDUCED MODULATIONAL INSTABILITY

The interplay of the optical Kerr effect and chromatic dispersion may lead to a large and diverse set of fascinating physical effects. A typical example of such effects is the phenomenon of modulational instability (MI): weak periodic perturbations of an intense carrier pump wave grow exponentially, leading to energy shedding of the pump wave into new frequencies within a certain spectral bandwidth [78–81]. Seeding the pump instability by the injection of a small-signal wave is commonly called induced-MI. In the temporal domain, induced-MI may lead to the breakup of a CW into ultrashort trains of pulses [82] with a repetition rate fixed by the signal frequency detuning from the pump wave. Another interesting application of MI is the frequency conversion of a single sideband signal, which, in the limit of weak conversion, yields phase conjugation. In this case, the MI process can be simply explained by considering the phenomenon as a four-photon mixing process, in which two pump photons are transferred to two symmetric sidebands (Stokes and anti-Stokes sidebands) whose frequencies are given by a phase matching condition [83]. Since in optical fibers the nonlinear coefficient is positive, the phase matching condition requires a negative GVD. Thus, scalar MI can only exist in the anomalous dispersion regime. However, scalar MI can also be observed for normal dispersion with different processes: first through the fourth-order dispersion with a negative coefficient [84–86], second through the boundary conditions of a cavity [87–89], and finally through periodic dispersion management [90–93]. Another mechanism that also leads to MI in the normal dispersion regime was first pointed out by Berkhoer and Zakharov, considering the nonlinear coupling between two different modes via cross-phase modulation [94]. Subsequently, several experiments with two orthogonal linear polarizations were performed in the normal dispersion regime, using either an isotropic fiber [95], a low-birefringence fiber [96,97], or a high-birefringence fiber [98,99]. This type of MI

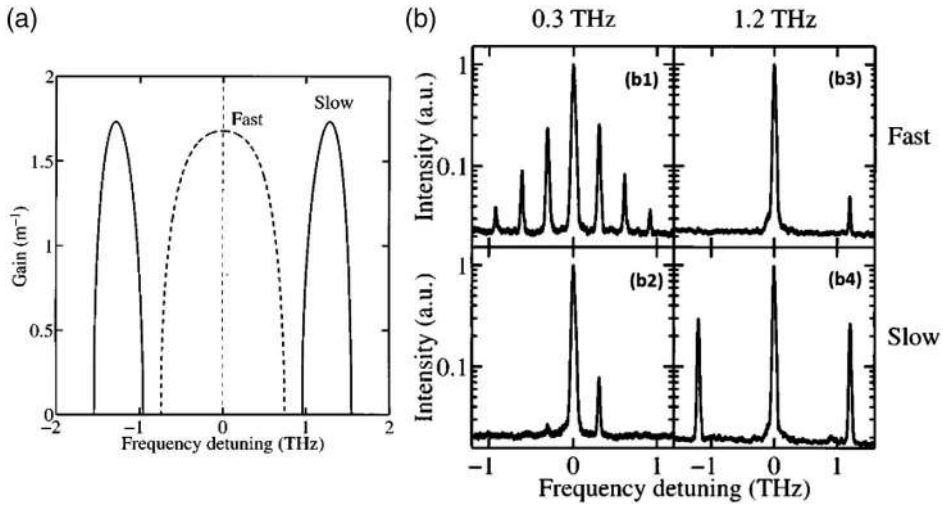

Fig. 8. (a) MPI gain versus sideband frequency detuning from a 112 W CW pump: solid (dashed) curve, pump on the slow (fast) axis. (b) Experimental spectra at the fiber output (on a logarithmic scale), with an input pump polarized along either (b1) the fast axis or (b3) the slow axis. The pump (signal) power is 112 (1.1) W, and the probe frequency detuning is 0.3 THz. (b2), (b4) As in parts (b1) and (b3) with a probe detuning of 1.2 THz (from [105]).

was also observed with two spatial modes of a slightly multimode fiber [100]. It is also possible to consider the nonlinear coupling between two pumps with different wavelengths and parallel states of polarization [101]. However, in this case MI has not been observed because of the simultaneous presence of FWM [102]. The situation is different if we consider two WDM pumps with orthogonal states of polarization. In this case, MI has been observed in the normal dispersion regime by using either two orthogonal linear polarization modes of relatively short samples of high-birefringence optical fibers [103] or two orthogonal circular polarization modes of short samples of isotropic fibers [104]. In fact, as the group velocity mismatch between the two orthogonal modes is large, the MI gain is narrowband, and the FWM among the two pumps is effectively suppressed.

Here, we review some results obtained on MI induced by cross-polarization modulation (XPolM-MI). From a theoretical point of view, XPolM-MI is directly derived by two coupled NLS equations [78]. In Subsection 3.A, we study the case of low-birefringence fibers, whereas in Subsection 3.B we discuss the case of high-birefringence fibers. Finally, in Subsection 3.C we consider the case of random birefringence fibers.

A. Polarization Modulation Instability in Low-Birefringence Fibers

1. Fast- and Slow-Axis Asymmetry

Polarization modulation instability (PMI) occurs when a strong pump wave launched on one axis of a relatively low-birefringence optical fiber generates a pair of Stokes and anti-Stokes sidebands that are polarized orthogonally to the pump wave. This process occurs in both dispersion regimes, and may exhibit widely different characteristics, depending on the polarization of the pump wave with respect to the optical fiber axes [96]. For example, in the normal-dispersion regime a pump beam can be modulationally unstable with its polarization along either the slow or fast axis, but in the latter case the input power must be larger than a threshold value P_t. On the other hand, the frequency dependence of the gain exhibits qualitatively different characteristics for fast and slow modes, as illustrated in Fig. 8 with a pump power $P_p = 112\ \text{W} = 1.6P_t$ and for the experimental conditions described in Ref. [105]. Here the solid and dashed curves were obtained for a pump aligned with the slow and the fast axes, respectively, of the ultralow-birefringence spun fiber. As can be seen in Fig. 8(a), a strong asymmetry appears between the fast and the slow modes. Indeed, in the case of fast-axis excitation the gain is almost flat for sideband detunings ranging from zero to a certain upper value determined by linear birefringence and pump power. Note that the fact that the MI gain curve extend at zero frequency is a signature of the fast-axis polarization instability [10]. On the other hand, for a pump aligned with the slow axis of the birefringent fiber, the PMI gain extends over a narrow band of frequencies ranging from a given frequency detuning that depends on linear birefringence to an upper frequency detuning that depends on both linear birefringence and pump power. The asymmetrical PMI behavior of the fast and slow axes was experimentally observed in relatively short samples of spun fibers by pumping either the fast or slow fiber axis with an intense pump beam weakly modulated by a small signal beam. Figure 8(b) shows the spectra observed at the fiber output when light was injected along each axis and with different signal frequency detunings. Here the pump and the signal powers were $P_p = 112$ W and $P_s = 1.1$ W, respectively. In Figs. 8(b1) and 8(b2) the pump was aligned with the fast axis, whereas in Figs. 8(b3) and 8(b4) the pump was oriented along the slow axis. Moreover, in Figs. 8(b1) and 8(b3) the signal frequency detuning was 0.3 THz, whereas in Figs. 8(b2) and 8(b4) this detuning was increased to 1.2 THz. As can be seen in Fig. 8(b1), with the small sideband detuning of 0.3 THz the fast fiber mode is modulationally unstable, in agreement with the theoretical predictions illustrated in Fig. 8(a). Moreover, Fig. 8(a) shows that the first harmonic of the initial modulation (at the frequency detuning of 0.6 THz) also falls within the gain band of PMI for the fast axis. The linear instability of the first harmonic is seeded by the FWM between the pump and the signal, which favors the conversion into further harmonics of higher order. On the other hand, Fig. 8(b) clearly shows that with slow-axis pumping the signal emerges from the fiber unamplified by the pump, and no significant idler wave is

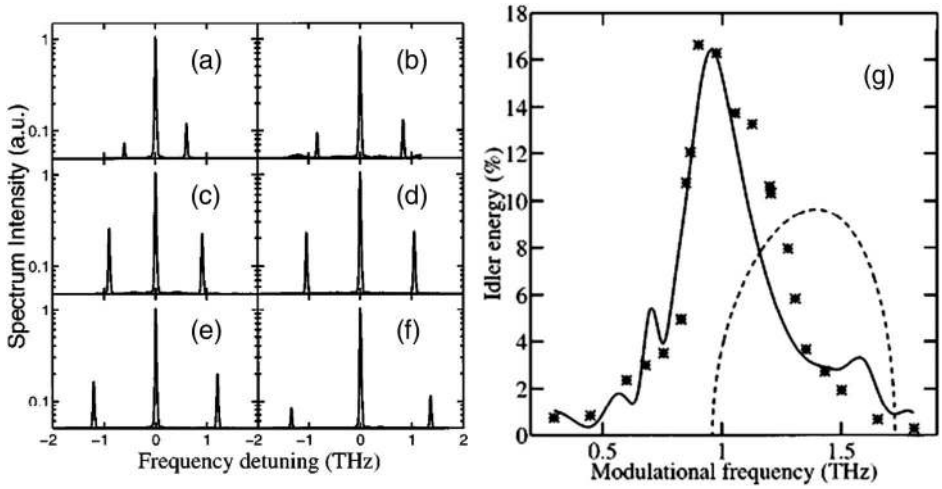

Fig. 9. Output experimental spectra for the peak pump power of 160 W and the pump signal detunings (in THz) (a) 0.6, (b) 0.825, (c) 0.9, (d) 1.047, (e) 1.2, and (f) 1.352. (g) Measured (symbols) and theoretical (solid curve) idler energy conversion versus pump signal detuning with pulsed waves for $P_p = 160$ W and $\alpha = 55\%$. Dashed curve, small signal MPI gain bandwidth (from [112]).

generated. Indeed, Fig. 8(a) shows that the slow mode is stable for the small sideband detuning of 0.3 THz. A similar situation occurs with fast-axis pumping and a relatively large detuning of 1.2 THz. Indeed, Fig. 8(b2) does not show any FWM gain whenever the pump is on the fast axis, again in agreement with the gain spectrum of Fig. 8(a). Finally, Fig. 8(b4) shows, in agreement with the theoretical prediction, that efficient mixing is recovered with slow-mode pumping. In this case, a deep polarization modulation of the pump wave is observed and no higher-order sidebands are generated, owing to the relatively narrow PMI gain curve of Fig. 8(a) (with slow-axis pumping).

Let us note that a theoretical investigation showed that PMI in low-bi fibers in the normal-GVD regime is also present for an arbitrary input polarization of the pump wave [106]. On the other hand, a convenient possibility of tuning the spectral profiles of PMI gain was demonstrated with a periodic evolution of the birefringence obtained by concatenating fibers with different linear beat lengths [107].

2. *Pump Depletion Effect*

In the frequency-domain description of the MI process, two pump photons are annihilated while a pair of downshifted and upshifted photons are created by the three-wave mixing parametric interaction in the fiber. The momentum conservation leads to wave-vector matching or to the so-called phase-matching condition, which determines the peak gain modulation. It is widely accepted that the phase-matching frequency also yields the maximum degree of frequency conversion. In other words, the MI peak gain frequency is identified with the optimal input signal detuning. However, Trillo and coworkers [108–113] have shown that this is only correct in the first stage of the propagation of the pump wave and for sufficiently weak input signals. Indeed, whenever the fiber length is such that a substantial fraction of pump energy is coupled into the sidebands, the optimal input signal detuning may strongly deviate from the usual MI small-signal predictions even for relatively weak (i.e., a few percent of the pump power) input signals [108–113]. The nonlinear stage or strongly depleted regime of PMI was investigated by injection of a signal orthogonally polarized with respect to the pump beam along the slow axis of a normally dispersive fiber. Under slow-axis pumping the parametric gain bandwidth is relatively narrow [see Fig. 8(a)], and higher-order sidebands can be neglected (three-wave mixing approximation). Hence, the depleted regime of PMI was described in this case by an integrable set of two coupled ordinary differential equations (three-wave model).

The efficiency of conversion of photons from the pump into both modulational sidebands versus signal detuning is displayed by the results given in Figs. 9(a)–9(f). More precisely, Fig. 9 shows a set of experimental spectra recorded for increasing values of the signal frequency detuning [112]. The peak pump power and the signal fraction are equal to 160 W and 5%, respectively. As can be seen in this figure, whenever the signal frequency detuning is increased progressively from 0.6 to 1.352 THz, the conversion increases rapidly when the modulation frequency is above 0.83 THz and decreases more slowly above 0.9 THz. This is in good agreement with theoretical predictions plotted in Fig. 9(g) together with experimental results. In fact, a global representation of the output idler energy fraction measured against the pump signal frequency detuning is shown in Fig. 9(g). In Fig. 9(g) the experimental data (stars) are compared with the predictions of the three-wave model (solid curve). The experimental data of Fig. 9(g) show that the highest idler energies (about 18%, corresponding to about 36% of pump depletion) are measured around 0.9 THz, which is substantially lower than the optimum frequency derived from the linear stability analysis $f_{\mathrm{opt}} = 1.4$ THz (phase matching frequency). Such enhancement of the frequency conversion for signal frequency detunings that lie outside the small-signal PMI gain spectrum (dashed curve) is a clear signature of the large-signal PMI. Indeed, in the undepleted-pump approximation the pump instability domain ranges from 0.96 to 1.72 THz, with a maximum gain at $f_{\mathrm{opt}} = 1.4$ THz. Figure 9(g) shows that the overall agreement between the three-wave model (solid curve) and the experimental data is very good.

In conclusion of this part, the studies of Trillo and coworkers clearly reveal that the strongest transfer of energy from the pump into the sidebands occurs outside the parametric gain bandwidth or, in other words, under conditions of

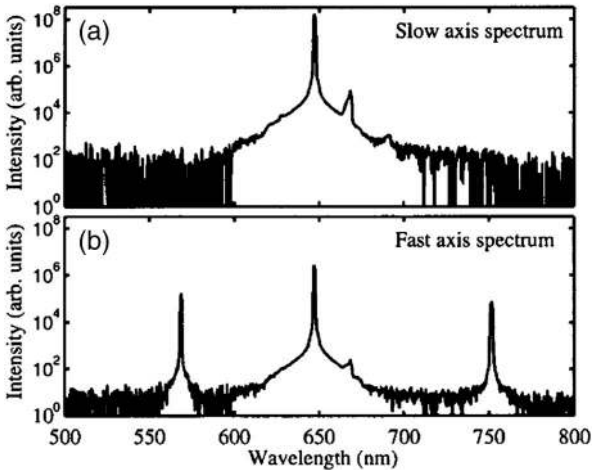

Fig. 10. Experimental output spectra emerging from (a) the slow axis and (b) the fast axis of 2 m of a PCF when the pump was linearly polarized along the slow axis. The peak power at the start of the PCF was 60 W. The intensity units have an arbitrary reference but accurately represent the relative intensity on each axis (from [116]).

modulational stability of the pump beam. This proves that the optimum signal frequency deviates significantly from the prediction of the linear stability analysis or the usual phase-matching argument. Therefore, the message we want to convey is that in the regime of strong frequency conversion (or strong pump energy depletion), one must not apply the usual formulas of phase matching for finding the frequency at which the MI gain is maximum. The second message we want to convey is that an efficient energy transfer from the pump to the two sidebands (about 20% in each sideband) could be achieved by using the process of polarization MI. Finally, we wish to note that similar properties have been observed using vector MI in high-birefringence fibers [114,115].

3. Polarization Modulation Instability in Photonic Crystal Fiber

Polarization modulation instability has been also observed in birefringent photonic crystal fibers (PCF) in the normal dispersion regime [116]. Figure 10 shows the spectrum of light on the slow [Fig. 10(a)] and the fast [Fig. 10(b)] axes emerging from the output end of the fiber, recorded for a peak pump power $P_p = 60$ W at the input. The pump was linearly polarized along the slow fiber axis. The two PMI sidebands can be clearly seen on the orthogonal fast fiber axis, as expected. The weak line observed at the right of the pump peak corresponds to the stimulated Raman peak at 13.2 THz from the pump frequency. But the most remarkable feature here is the large frequency shift of 64 THz between the generated frequencies and the pump frequency. This large value of the frequency shift, when compared with that obtained in the previous experiments (see Fig. 8), is due to the smaller value of the dispersion and the higher value of the phase birefringence. This performance was possible thanks to the extraordinary dispersion engineering properties offered by PCFs [117].

B. Modulation Instability Induced by Cross-Polarization Modulation in High-Birefringence Fibers

1. Generation of Vector Dark Soliton Trains

As mentioned above, induced MI may lead in the time domain to the breakup of a quasi-CW pump wave into a train of ultrashort pulses [118,119]. The repetition rate of the pulses is given by the modulational frequency, which is equal to the detuning between the signal and the pump waves. The temporal shape of these ultrashort pulses depends not only on the powers of the different waves but also on the modulational frequency [105]. In particular, trains of dark solitons with a terahertz repetition rate have been generated by modulational instability induced by cross-polarization modulation (XPolM-MI) in ultralow birefringence optical fibers [120]. Moreover, families of vector dark soliton solutions were found for the coupled NLS equations that apply to highly birefringent (hi-bi) fibers [121].

By exploiting hi-bi fibers operating in the normal dispersion regime, it has also been possible to observe vector MI as well as the generation of vector dark soliton trains at repetition rates of 2.5 THz [122,123]. The fiber used in the experiments of Seve *et al.* was a 1.8 m length of hi-bi fiber, equally pumped on the fast and slow axes by a 56 W peak power wave. MI was induced by injecting on the slow axis a weak 2.1 W peak power signal with a 2.5 THz detuning from the pump. The technique of frequency-resolved optical gating (FROG) was used to completely characterize the intensity and phase of the dark soliton trains [124,125]. Figures 11(a) and 11(b) show, respectively, the measured and retrieved FROG traces of the emerging light from the slow axis, and the solid lines in Fig. 11(c) show the corresponding spectrum. The retrieved intensity and phase are shown by the lines in Fig. 11(d). Let us remark that the retrieved intensity profile does not exhibit 100% modulation, but a reduced modulation depth of 96%, so that the solitons must be interpreted as "gray" rather than "black." It is significant that this reduced modulation depth is also manifested in the characteristics of the phase shift which is observed across the center of the dark soliton. In the case of 100% modulated black solitons, an

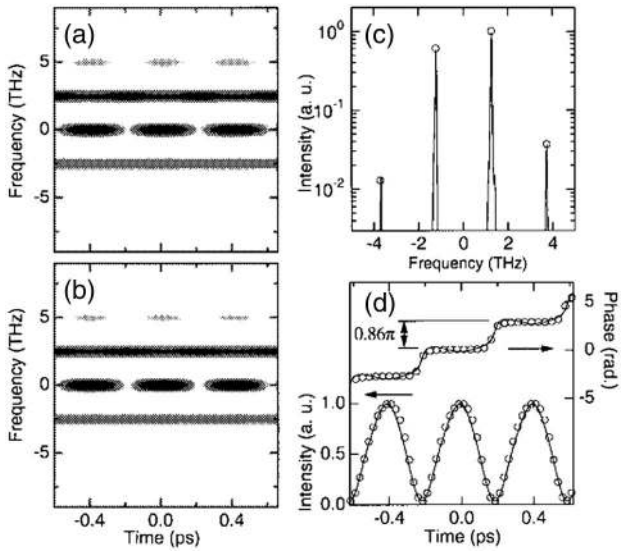

Fig. 11. (a) Measured and (b) retrieved SHG-FROG traces of the dark soliton train at 2.5 THz. (c) Measured spectrum (lines) compared with that calculated from the retrieved pulse train (circles). (d) The solid lines show the retrieved intensity (left axis) and phase (right axis), while the circles show the expected results from coupled NLSE simulations. With the frequency axis used in the figure, zero frequency corresponds to the mean frequency of the pump and signal waves (from [125]).

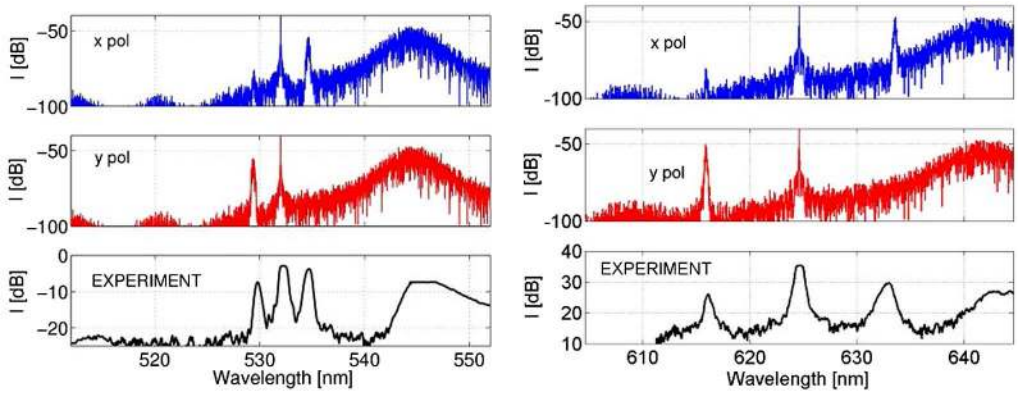

Fig. 12. Calculated (upper curves) and measured polarization sidebands for two pump wavelengths equal respectively to 532 nm (left) and 625 nm (right) (from [127]).

abrupt phase jump of π is expected, but gray solitons are associated with a continuously varying phase shift of reduced magnitude [78]. The retrieved phase in Fig. 11(d) confirms this expected behavior, showing a phase shift of 0.86π across the center of the dark soliton. Numerical simulations of these experiments, based on two incoherently coupled NLS equations, are shown by circles in Fig. 11(d). The simulation results are in good agreement with the measured results, particularly with respect to the 96% modulation depth and the phase shift.

An interesting feature of the dark solitons is their reduced sensitivity, with respect to bright solitons, to mutual interactions and amplifier-noise timing jitter [126].

2. *Frequency Tunable Modulational Instability in Photonic Crystal Fibers*

In the context of the generation of new frequencies or parametric amplification, it is very interesting to be able to easily adjust the frequencies of the sidebands generated by modulation instability to satisfy the specific needs of new laser frequencies for novel experiments or applications. Among the various methods which were proposed so far, the shift of the pump wavelength [127] or pressure-induced changes in the linear properties of a PCF [128] seem to be the most promising.

For the first approach, the authors of Ref. [127] reported experimental investigations of the frequency tuning properties of XPolM-MI in a PCF, and thus demonstrated sideband shifts in the range of 2.6–8.5 THz by shifting the pump wavelength from 532 to 625 nm. In their experiments the authors used nanosecond pulses to ensure full temporal overlap between the pump and the sidebands throughout the whole 5 m long sample of the PCF. The peak power of the pulses in the fiber was kept constant and equal to 30–40 W. In order to observe XPolM-MI in the high-birefringence PCF, the pump beam was linearly polarized and aligned at 45° with respect to the fiber polarization axes. Under these conditions, orthogonally polarized sidebands were generated. The black solid curves in Fig. 12 show the spectra recorded without polarization discrimination with a pump wavelength of 532 and 625 nm, left and right side of Fig. 12, respectively. Figure 12 also shows a comparison of the experimental spectra with numerical solutions of the incoherently coupled NLS equations. Here, blue and red spectra are associated respectively with x- and y-polarized components of the output field. Let us note that the orthogonal polarization of XPolM-MI sidebands was confirmed by the experiments. The results of Fig. 12 show an excellent agreement between theory and experiments. The observed polarization sideband detuning grew from 2.6 THz with a pump at 532 nm up to 8.5 THz with a pump wavelength of 625 nm. These observations show that the strong frequency-dependent linear propagation characteristics of guided modes in PCFs may be used to obtain a flexible source of parametric gain and broadly frequency tunable waves.

In the second case, the authors investigated the vector and scalar frequency conversion processes in an externally tuned microstructured fiber. Let us note that the coexistence of scalar and vector MI has been also observed in PCF with normal dispersion [129]. In particular, the impact of hydrostatic pressure on MI gain bands was studied [128]. Their experimental results show that scalar MI is insensitive to hydrostatic pressure, while the XPolM-MI strongly depends on pressure. This difference in behavior comes from the different nonlinear phase-matching relations. Experimental measurements were well reproduced by numerical simulations based on coupled nonlinear Schrödinger equations corresponding to both polarization modes. The simulations presented in Fig. 13 take into account the longitudinal distribution of the modal birefringence induced by the hydrostatic pressure. Figure 13 shows typical spectra obtained for different pressures applied to the fiber. The simulations show high sensitivity of the vector MI sidebands against variations of the hydrostatic

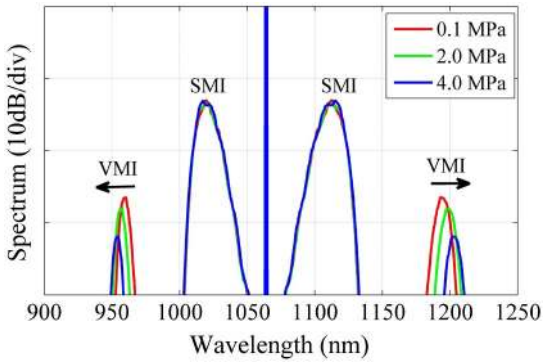

Fig. 13. Output spectra obtained from numerical simulations for different values of pressure applied to the central part of the fiber. Arrows indicate the expected shift direction of the vector MI bands (from [128]).

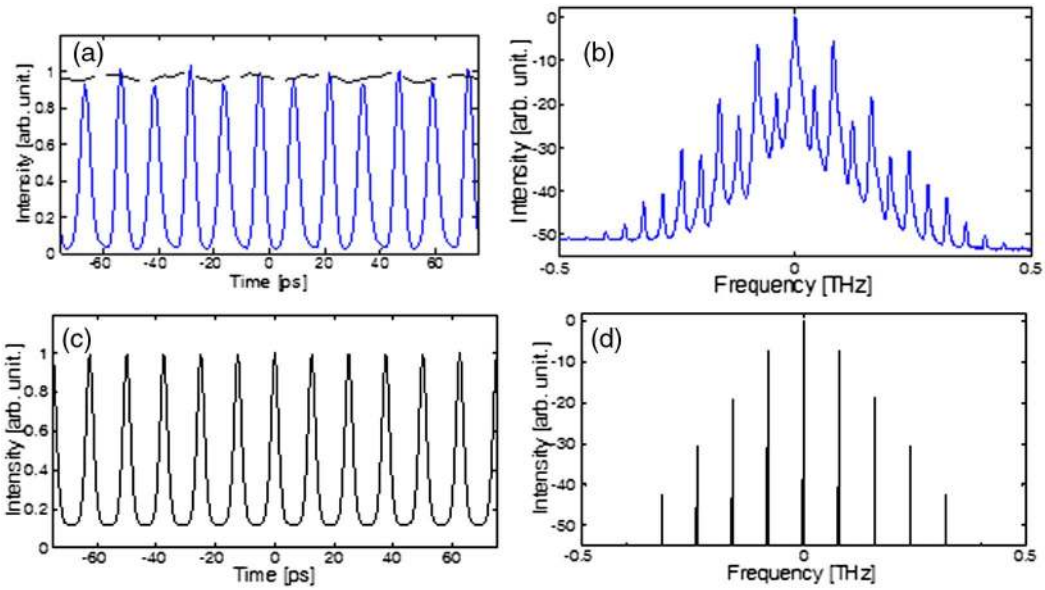

Fig. 14. (a) Experimental temporal profiles at the input (dashed line) and output (solid line) of the fiber for orthogonal polarized pump and signal. (b) Associated experimental spectrum. The output polarizer was oriented parallel to the pump polarization. (c) Temporal and (d) spectral profiles obtained from numerical simulations when the pump and signal waves are injected with orthogonal polarizations (from [131]).

pressure applied to the fiber, while the scalar MI sidebands are pressure independent. These results prove that frequency conversion by means of XPolM-MI in microstructured fibers is well suited for pressure-sensing applications [128].

C. Modulation Instability Induced by Cross-Polarization Modulation in Randomly Birefringent Fibers

In the field of high-speed optical communications it is relevant to design new methods to increase the repetition rates of laser sources, well beyond the capabilities of electrically driven modulators. In this context, the efficient conversion of a modulated wave into a nearly sinusoidally modulated wave at harmonic frequencies has been demonstrated by means of XPolM-MI induced by multiple FWM in the case of a normally dispersive, highly birefringent fiber at visible wavelengths [130]. Furthermore, a recent work [131] has focused on XPolM-MI in the anomalous dispersion regime of a randomly birefringent fiber, where the self- and cross-induced nonlinear terms have the same weight (Manakov system [35]). This configuration applies to the relevant practical case of telecommunication fiber-optic links with random birefringence [36].

In Ref. [131], pump and signal waves were injected with orthogonal linear polarization states into a 5.1 km telecom fiber with low PMD (0.02 ps/km$^{1/2}$). The pump average power was fixed to 20.5 dBm, whereas the signal power on the orthogonal axis was set to 10.5 dBm. The pump signal detuning (i.e., the initial modulation frequency) was fixed to 40 GHz. Figures 14(a) and 14(b) show the temporal and spectral profiles of the light exiting the optical fiber along the polarization direction of the emerging pump wave. As can be seen in Fig. 14, the spectrum is dominated by even harmonics at multiple frequencies of 80 GHz, whereas no exponential growth of the initial modulation is observed at 40 GHz. This interesting phenomenon only appears if the initial frequency modulation is fixed at about half of the peak gain frequency of scalar MI ($\Omega_{MI}/2 = 40$ GHz). As shown in Fig. 14(a), this spectral characteristic corresponds, in the time domain, to a pulse at twice the frequency of the initial signal frequency, i.e., the second harmonic at 80 GHz, in good qualitative agreement with the numerical solutions of the Manakov equations [see Figs. 14(c) and 14(d)].

4. CONCLUSIONS

In this mini-review, we highlighted the remarkable phenomenon of polarization attraction which, in our opinion, should find many applications in nonlinear optics and possibly in other domains of physics and technology. Indeed, practical CW power level fiber-optic devices based on either lossless or dissipative polarization attraction have been enabled in recent years by the availability of low-PMD telecom optical fibers. We also presented the MI process which exploits the SOP of light. In particular, we pointed out the regime of high-energy conversion for which conventional nonlinear phase matching can no longer be applied. We have also identified some applications of the process, such as the generation of dark solitons at high repetition rate, the frequency conversion with very large frequency shifts, the ability to generate new waves with wavelength tunability, and finally, the possibility of doubling the rate of high-speed laser sources. As a perspective for further work, let us mention the possibility of using composite birefringence PCFs, i.e., with both geometry and stress-induced birefringence, which permit the independent management of the wavelength dependence of both phase and group birefringence [132]. This opens the way to new scenarios for vector modulational instabilities, e.g., by using a PCF with zero phase birefringence (as in an isotropic standard fiber) and, simultaneously, large group birefringence (as in a hi-bi standard fiber).

ACKNOWLEDGMENTS

This work was carried out with support from the Italian Ministry of University and Research (MIUR) through grant

2008MPSSNX, the Conseil Régional de Bourgogne, the Labex ACTION program (contract ANR-11-LABX-01-01), and the iXCore Foundation.

REFERENCES

1. J. E. Heebner, R. S. Bennink, R. W. Boyd, and R. A. Fisher, "Conversion of unpolarized light to polarized light with greater than 50% efficiency by photorefractive two-beam coupling," Opt. Lett. **25**, 257–259 (2000).
2. S. Pitois and M. Haelterman, "Optical fiber polarization funnel," in *Nonlinear Guided Waves and Their Applications*, OSA Technical Digest Series (Optical Society of America, 2001), paper MC79, pp. 278–280.
3. A. E. Kaplan, "Light-induced nonreciprocity, field invariants, and nonlinear eigenpolarizations," Opt. Lett. **8**, 560–562 (1983).
4. A. E. Kaplan and C. T. Law, "Isolas in four-wave mixing optical bistability," IEEE J. Quantum Electron. **21**, 1529–1537 (1985).
5. D. J. Gauthier, M. S. Malcuit, A. L. Gaeta, and R. W. Boyd, "Polarization bistability of counterpropagating laser beams," Phys. Rev. Lett. **64**, 1721–1724 (1990).
6. G. Gregori and S. Wabnitz, "New exact solutions and bifurcations in the spatial distribution of polarization in third-order nonlinear optical interactions," Phys. Rev. Lett. **56**, 600–603 (1986).
7. S. Wabnitz and G. Gregori, "Symmetry-breaking and intrinsic polarization instability in degenerate four-wave mixing," Opt. Commun. **59**, 72–76 (1986).
8. S. Trillo and S. Wabnitz, "Intermittent spatial chaos for counterpropagating beams in a birefringent optical fiber," Phys. Rev. A **36**, 3881–3884 (1987).
9. D. David, D. D. Holm, and M. V. Tratnik, "Hamiltonian chaos in nonlinear optical polarization dynamics," Phys. Rep. **187**, 281–367 (1990).
10. S. Trillo, S. Wabnitz, R. H. Stolen, G. Assanto, C. T. Seaton, and G. I. Stegeman, "Experimental observation of polarization instability in a birefringent optical fiber," Appl. Phys. Lett. **49**, 1224–1226 (1986).
11. A. L. Gaeta, R. W. Boyd, J. R. Ackerhalt, and P. W. Milonni, "Instabilities and chaos in the polarizations of counterpropagating light fields," Phys. Rev. Lett. **58**, 2432–2435 (1987).
12. V. E. Zakharov and A. V. Mikhailov, "Polarization domains in nonlinear optics," JETP Lett. **45**, 349–352 (1987).
13. A. V. Mikhailov and S. Wabnitz, "Polarization dynamics of counterpropagating beams in optical fibers," Opt. Lett. **15**, 1055–1057 (1990).
14. M. V. Tratnik and J. E. Sipe, "Polarization solitons," Phys. Rev. Lett. **58**, 1104–1107 (1987).
15. S. Wabnitz, "Chiral polarization solitons in elliptically birefringent spun optical fibers," Opt. Lett. **34**, 908–910 (2009).
16. S. Wabnitz, "Cross-polarization modulation domain wall solitons for WDM signals in birefringent optical fibers," IEEE Photon. Technol. Lett. **21**, 875–877 (2009).
17. S. Wabnitz and B. Daino, "Polarization domains and instabilities in nonlinear optical fibers," Phys. Lett. A **182**, 289–293 (1993).
18. S. Pitois, G. Millot, and S. Wabnitz, "Polarization domain wall solitons with counterpropagating laser beams," Phys. Rev. Lett. **81**, 1409–1412 (1998).
19. S. Pitois, G. Millot, and S. Wabnitz, "Nonlinear polarization dynamics of counterpropagating waves in an isotropic optical fiber: theory and experiments," J. Opt. Soc. Am. B **18**, 432–443 (2001).
20. A. B. Aceves and S. Wabnitz, "Self-induced transparency solitons in nonlinear refractive periodic optical media," Phys. Lett. A **141**, 37–42 (1989).
21. V. V. Kozlov and S. Wabnitz, "Instability of optical solitons in the boundary value problem for a medium of finite extension," Lett. Math. Phys. **96**, 405–413 (2011).
22. E. Assemat, A. Picozzi, H. R. Jauslin, and D. Sugny, "Instabilities of optical solitons and Hamiltonian singular solutions in a medium of finite extension," Phys. Rev. A **84**, 013809 (2011).
23. S. Pitois, A. Sauter, and G. Millot, "Simultaneous achievement of polarization attraction and Raman amplification in isotropic optical fibers," Opt. Lett. **29**, 599–601 (2004).
24. S. Pitois, A. Picozzi, G. Millot, H. R. Jauslin, and M. Haelterman, "Polarization and modal attractors in conservative counterpropagating four-wave interaction," Europhys. Lett. **70**, 88–94 (2005).
25. S. Pitois, J. Fatome, and G. Millot, "Polarization attraction using counter-propagating waves in optical fiber at telecommunication wavelengths," Opt. Express **16**, 6646–6651 (2008).
26. J. Fatome, S. Pitois, P. Morin, and G. Millot, "Observation of light-by-light polarization control and stabilization in optical fibre for telecommunication applications," Opt. Express **18**, 15311–15317 (2010).
27. J. Fatome, P. Morin, S. Pitois, and G. Millot, "Light-by-light polarization control of 10-Gb/s RZ and NRZ telecommunication signals," IEEE J. Sel. Top. Quantum Electron. **18**, 621–628 (2012).
28. V. V. Kozlov, J. Nuño, and S. Wabnitz, "Theory of lossless polarization attraction in telecommunication fiber," J. Opt. Soc. Am. B **28**, 100–108 (2011).
29. V. V. Kozlov, J. Nuño, and S. Wabnitz, "Theory of lossless polarization attraction in telecommunication fibers: erratum," J. Opt. Soc. Am. B **29**, 153–154 (2012).
30. E. Assémat, A. Picozzi, H. R. Jauslin, and D. Sugny, "Hamiltonian tools for the analysis of optical polarization system," J. Opt. Soc. Am. B **29**, 559–571 (2012).
31. D. Sugny, A. Picozzi, S. Lagrange, and H. R. Jauslin, "On the role of singular tori in the spatio-temporal dynamics of nonlinear wave systems," Phys. Rev. Lett. **103**, 034102 (2009).
32. S. Lagrange, D. Sugny, A. Picozzi, and H. R. Jauslin, "Singular-tori as attractors of four-wave-interaction systems," Phys. Rev. E **81**, 016202 (2010).
33. E. Assémat, S. Lagrange, A. Picozzi, H. R. Jauslin, and D. Sugny, "Complete nonlinear polarization control in an optical fiber system," Opt. Lett. **35**, 2025–2027 (2010).
34. K. S. Turitsyn and S. Wabnitz, "Stability analysis of polarization attraction in optical fibers," Opt. Commun. **307**, 62–66 (2013).
35. S. V. Manakov, "On the theory of two-dimensional stationary self focussing of electromagnetic waves," Sov. Phys. J. Exp. Theor. Phys. **38**, 248–253 (1974).
36. P. K. A. Wai and C. R. Menyuk, "Polarization mode dispersion, decorrelation, and diffusion in optical fibers with randomly varying birefringence," J. Lightwave Technol. **14**, 148–157 (1996).
37. D. Marcuse, C. R. Menyuk, and P. K. A. Wai, "Application of the Manakov-PMD equation to studies of signal propagation in optical fibers with randomly varying birefringence," J. Lightwave Technol. **15**, 1735–1746 (1997).
38. M. Barozzi and A. Vannucci, "Performance characterization and guidelines for the design of a counter-propagating nonlinear lossless polarizer," J. Opt. Soc. Am. B **30**, 3102–3110 (2013).
39. P. Morin, J. Fatome, C. Finot, S. Pitois, R. Claveau, and G. Millot, "All-optical nonlinear processing of both polarization state and intensity profile for 40 Gbit/s regeneration applications," Opt. Express **19**, 17158–17166 (2011).
40. J. Fatome, D. Sugny, S. Pitois, P. Morin, M. Guasoni, A. Picozzi, H. R. Jauslin, C. Finot, G. Millot, and S. Wabnitz, "All-optical regeneration of polarization of a 40-Gbit/s return-to-zero telecommunication signal," Photon. Res. **1**, 115–123 (2013).
41. J. Fatome, S. Pitois, P. Morin, E. Assémat, D. Sugny, A. Picozzi, H. R. Jauslin, G. Millot, V. V. Kozlov, and S. Wabnitz, "A universal optical all-fiber omnipolarizer," Sci. Rep. **2**, 938–946 (2012).
42. V. V. Kozlov, J. Fatome, P. Morin, S. Pitois, G. Millot, and S. Wabnitz, "Nonlinear repolarization dynamics in optical fibers: transient polarization attraction," J. Opt. Soc. Am. B **28**, 1782–1791 (2011).
43. V. V. Kozlov, J. Fatome, P. Morin, S. Pitois, and S. Wabnitz, "Nonlinear optical fiber polarization tracking at 200 krad/s," *37th European Conference on Optical Communication (ECOC)*, Geneva, Switzerland, September 18–22, 2011.
44. V. V. Kozlov and S. Wabnitz, "Theoretical study of polarization attraction in high-birefringence and spun fibers," Opt. Lett. **35**, 3949–3951 (2010).
45. E. Assémat, D. Dargent, A. Picozzi, H. R. Jauslin, and D. Sugny, "Polarization control in spun and telecommunication optical fibers," Opt. Lett. **36**, 4038–4040 (2011).

46. V. V. Kozlov, K. Turitsyn, and S. Wabnitz, "Nonlinear repolarization in optical fibers: polarization attraction with copropagating beams," Opt. Lett. **36**, 4050–4052 (2011).
47. V. V. Kozlov, M. Barozzi, A. Vannucci, and S. Wabnitz, "Lossless polarization attraction of co-propagating beams in telecom fibers," J. Opt. Soc. Am. B **30**, 530–540 (2013).
48. M. Guasoni, E. Assémat, P. Morin, A. Picozzi, J. Fatome, S. Pitois, H. R. Jauslin, G. Millot, and D. Sugny, "Line of polarization attraction in highly birefringent optical fibers," J. Opt. Soc. Am. B **31**, 572–579 (2014).
49. P.-Y. Bony, M. Guasoni, E. Assémat, S. Pitois, D. Sugny, A. Picozzi, H. R. Jauslin, and J. Fatome, "Optical flip-flop memory and data packet switching operation based on polarization bistability in a telecommunication optical fiber," J. Opt. Soc. Am. B **30**, 2318–2325 (2013).
50. R. H. Stolen, "Polarization effects in fiber Raman and Brillouin lasers," IEEE J. Quantum Electron. **15**, 1157–1160 (1979).
51. M. Martinelli, M. Cirigliano, M. M. Ferrario, L. Marazzi, and P. Martelli, "Evidence of Raman-induced polarization pulling," Opt. Express **17**, 947–955 (2009).
52. L. Ursini, M. Santagiustina, and L. Palmieri, "Raman nonlinear polarization pulling in the pump depleted regime in randomly birefringent fibers," IEEE Photon. Technol. Lett. **23**, 254–256 (2011).
53. V. V. Kozlov, J. Nuño, J. D. Ania-Castañón, and S. Wabnitz, "Theory of fiber optic Raman polarizers," Opt. Lett. **35**, 3970–3972 (2010).
54. V. V. Kozlov, J. Nuño, J. D. Ania-Castañón, and S. Wabnitz, "Theoretical study of optical fiber Raman polarizers with counterpropagating beams," J. Lightwave Technol. **29**, 341–347 (2011).
55. V. V. Kozlov and S. Wabnitz, "Suppression of relative intensity noise in fiber-optic Raman polarizers," IEEE Photon. Technol. Lett. **23**, 1088–1090 (2011).
56. V. V. Kozlov, J. Nuño, J. D. Ania-Castañón, and S. Wabnitz, "Multi-channel Raman polarizer with suppressed relative intensity noise for WDM transmission lines," Opt. Lett. **37**, 2073–2075 (2012).
57. V. Kozlov, J. Nuño, J. D. Ania-Castañón, and S. Wabnitz, "Analytic theory of fiber-optic Raman polarizers," Opt. Express **20**, 27242–27247 (2012).
58. Q. Lin and G. P. Agrawal, "Vector theory of stimulated Raman scattering and its application to fiber-based Raman amplifiers," J. Opt. Soc. Am. B **20**, 1616–1631 (2003).
59. S. Sergeyev, S. Popov, and A. T. Friberg, "Spun fiber Raman amplifiers with reduced polarization impairments," Opt. Express **16**, 14380–14389 (2008).
60. F. Chiarello, L. Palmieri, M. Santagiustina, R. Gamatham, and A. Galtarossa, "Experimental characterization of the counterpropagating Raman polarization attraction," Opt. Express **20**, 26050 (2012).
61. F. Chiarello, L. Ursini, L. Palmieri, and M. Santagiustina, "Polarization attraction in counterpropagating fiber Raman amplifiers," IEEE Photon. Technol. Lett. **23**, 1457–1459 (2011).
62. S. V. Sergeyev, "Activated polarization pulling and decorrelation of signal and pump states of polarization in a fiber Raman amplifier," Opt. Express **19**, 24268–24279 (2011).
63. S. Sergeyev and S. Popov, "Two-section fiber optic Raman polarizer," IEEE J. Quantum Electron. **48**, 56–60 (2012).
64. S. Sergeyev, "Fiber Raman amplification in a two-scale spun fiber," Opt. Mater. Express **2**, 1683–1689 (2012).
65. A. Zadok, E. Zilka, A. Eyal, L. Thévenaz, and M. Tur, "Vector analysis of stimulated Brillouin scattering amplification in standard single-mode fibers," Opt. Express **16**, 21692–21707 (2008).
66. J. Fatome, S. Pitois, and G. Millot, "Experimental evidence of Brillouin-induced polarization wheeling in highly birefringent optical fibers," Opt. Express **17**, 12612 (2009).
67. Z. Shmilovitch, N. Primerov, A. Zadok, A. Eyal, S. Chin, L. Thévenaz, and M. Tur, "Dual-pump push-pull polarization control using stimulated Brillouin scattering," Opt. Express **19**, 25873–25880 (2011).
68. M. Guasoni and S. Wabnitz, "Nonlinear polarizers based on four-wave mixing in high-birefringence optical fibers," J. Opt. Soc. Am. B **29**, 1511–1520 (2012).
69. Q. Lin and G. P. Agrawal, "Vector theory of four-wave mixing: polarization effects in fiber-optic parametric amplifiers," J. Opt. Soc. Am. B **21**, 1216–1224 (2004).
70. Q. Lin and G. P. Agrawal, "Effects of polarization-mode dispersion on fiber-based parametric amplification and wavelength conversion," Opt. Lett. **29**, 1114–1116 (2004).
71. C. McKinstrie, H. Kogelnik, R. Jopson, S. Radic, and A. Kanaev, "Four-wave mixing in fibers with random birefringence," Opt. Express **12**, 2033–2055 (2004).
72. J. F. L. Freitas, C. J. S. de Matos, M. B. Costa e Silva, and A. S. L. Gomes, "Impact of phase modulation and parametric gain on signal polarization in an anomalously dispersive optical fiber," J. Opt. Soc. Am. B **24**, 1469–1474 (2007).
73. M. Guasoni, V. V. Kozlov, and S. Wabnitz, "Theory of polarization attraction in parametric amplifiers based on telecommunication fibers," J. Opt. Soc. Am. B **29**, 2710–2720 (2012).
74. B. Stiller, P. Morin, D. M. Nguyen, J. Fatome, S. Pitois, E. Lantz, H. Maillotte, C. R. Menyuk, and T. Sylvestre, "Demonstration of polarization pulling using a fiber-optic parametric amplifier," Opt. Express **20**, 27248–27253 (2012).
75. S. Trillo and S. Wabnitz, "Parametric and Raman amplification in birefringent fibers," J. Opt. Soc. Am. B **9**, 1061–1082 (1992).
76. N. Muga, M. Ferreira, and A. Pinto, "Broadband polarization pulling using Raman amplification," Opt. Express **19**, 18707–18712 (2011).
77. P. Morin, S. Pitois, and J. Fatome, "Simultaneous polarization attraction and Raman amplification of a light beam in optical fibers," J. Opt. Soc. Am. B **29**, 2046–2052 (2012).
78. G. P. Agrawal, *Nonlinear Fiber Optics*, 5th ed. (Academic, 2013).
79. V. I. Bespalov and V. I. Talanov, "Filamentary structures of light beams in nonlinear liquids," J. Exp. Theor. Phys. Lett. **3**, 307–310 (1966).
80. T. B. Benjamin and J. E. Feir, "The designation of wave-trains on deep water, Part 1, Theory," J. Fluid Mech. **27**, 417–430 (1967).
81. A. Hasegawa and W. F. Brinkman, "Tunable coherent IR and FIR sources utilizing modulational instability," IEEE J. Quantum Electron. **16**, 694–697 (1980).
82. K. Tai, A. Hasegawa, and A. Tomita, "Observation of modulational instability in optical fibers," Phys. Rev. Lett. **56**, 135–138 (1986).
83. R. H. Stolen, M. A. Bosch, and C. Lin, "Phase matching in birefringent fibers," Opt. Lett. **6**, 213–215 (1981).
84. F. K. Abdullaev, S. A. Darmanyan, S. Bischoff, P. L. Christiansen, and M. P. Sorensen, "Modulational instability in optical fibers near the zero dispersion point," Opt. Commun. **108**, 60–64 (1994).
85. S. Pitois and G. Millot, "Experimental observation of a new modulational instability spectral window induced by fourth-order dispersion in a normally dispersive single-mode optical fiber," Opt. Commun. **226**, 415–422 (2003).
86. J. D. Harvey, R. Leonhardt, S. Coen, G. K. L. Wong, J. C. Knight, W. J. Wadsworth, and P. St. J. Russell, "Scalar modulation instability in the normal dispersion regime by use of a photonic crystal fiber," Opt. Lett. **28**, 2225–2227 (2003).
87. M. Haelterman, S. Wabnitz, and S. Trillo, "Additive-modulation-instability ring laser in the normal dispersion regime of a fiber," Opt. Lett. **17**, 745–747 (1992).
88. S. Coen and M. Haelterman, "Modulational Instability induced by cavity boundary conditions in a normally dispersive optical fiber," Phys. Rev. Lett. **79**, 4139–4142 (1997).
89. T. Sylvestre, S. Coen, P. Emplit, and M. Haelterman, "Self-induced modulational instability laser revisited: normal dispersion and dark-pulse train generation," Opt. Lett. **27**, 482–484 (2002).
90. F. Matera, A. Mecozzi, M. Romagnoli, and M. Settembre, "Sideband instability induced by periodic power variation in long-distance fiber links," Opt. Lett. **18**, 1499–1501 (1993).
91. A. Armaroli and F. Biancalana, "Tunable modulational instability sidebands via parametric resonance in periodically tapered optical fibers," Opt. Express **20**, 25096–25110 (2012).
92. M. Droques, A. Kudlinski, G. Bouwmans, G. Martinelli, and A. Mussot, "Experimental demonstration of modulation instability

in an optical fiber with a periodic dispersion landscape," Opt. Lett. **37**, 4832–4834 (2012).
93. M. Droques, A. Kudlinski, G. Bouwmans, G. Martinelli, and A. Mussot, "Dynamics of the modulation instability spectrum in optical fibers with oscillating dispersion," Phys. Rev. A **87**, 013813 (2013).
94. A. L. Berkhoer and V. E. Zakharov, "Self excitation of waves with different polarizations in nonlinear media," Sov. Phys. J. Exp. Theor. Phys. **31**, 486–490 (1970).
95. P. Kockaert, M. Haelterman, S. Pitois, and G. Millot, "Isotropic polarization modulational instability and domain walls in spun fibers," Appl. Phys. Lett. **75**, 2873–2875 (1999).
96. S. Wabnitz, "Modulational polarization instability of light in a nonlinear birefringent dispersive medium," Phys. Rev. A **38**, 2018–2021 (1988).
97. G. Millot, E. Seve, and S. Wabnitz, "Polarization symmetry breaking and pulse train generation from the modulation of light waves," Phys. Rev. Lett. **79**, 661–664 (1997).
98. J. E. Rothenberg, "Modulational instability for normal dispersion," Phys. Rev. A **42**, 682–685 (1990).
99. P. D. Drummond, T. A. B. Kennedy, J. M. Dudley, R. Leonhardt, and J. D. Harvey, "Cross-phase modulational instability in high-birefringence fibers," Opt. Commun. **78**, 137–142 (1990).
100. G. Millot, S. Pitois, P. Tchofo Dinda, and M. Haelterman, "Observation of modulational instability induced by velocity-matched cross-phase modulation in a normally dispersive bimodal fiber," Opt. Lett. **22**, 1686–1688 (1997).
101. G. P. Agrawal, "Modulation instability induced by cross-phase modulation," Phys. Rev. Lett. **59**, 880–883 (1987).
102. A. Armaroli and S. Trillo, "Modulational instability due to cross-phase modulation versus multiple four-wave mixing: the normal dispersion regime," J. Opt. Soc. Am. B **31**, 551–558 (2014).
103. E. Seve, P. Tchofo Dinda, G. Millot, M. Remoissenet, J. M. Bilbault, and M. Haelterman, "Modulational instability and critical regime in a highly birefringent fiber," Phys. Rev. A **54**, 3519–3534 (1996).
104. G. Millot, S. Pitois, and P. Tchofo Dinda, "Modulational instability processes in optical isotropic fibers under dual-frequency circular polarization pumping," J. Opt. Soc. Am. B **19**, 454–460 (2002).
105. G. Millot, E. Seve, S. Wabnitz, and M. Haelterman, "Observation of induced modulational polarization instabilities and pulse-train generation in the normal-dispersion regime of a birefringent optical fiber," J. Opt. Soc. Am. B **15**, 1266–1277 (1998).
106. S. Trillo and S. Wabnitz, "Bloch wave theory of modulational polarization instabilities in birefringent optical fibers," Phys. Rev. E **56**, 1048–1058 (1997).
107. S. G. Murdoch, M. D. Thomson, R. Leonhardt, J. D. Harvey, and T. B. Kennedy, "Quasi-phase matching in an optical fiber with periodic birefringence," J. Opt. Soc. Am. B **14**, 1816–1822 (1997).
108. G. Cappellini and S. Trillo, "Third-order three-wave mixing in single-mode fibers: exact solutions and spatial instability effects," J. Opt. Soc. Am. B **8**, 824–838 (1991).
109. G. Cappellini and S. Trillo, "Bifurcations and 3-wave-mixing instabilities in nonlinear propagation in birefringent dispersive media," Phys. Rev. A **44**, 7509–7523 (1991).
110. S. Trillo and S. Wabnitz, "Dynamics of the nonlinear modulational instability in optical fibers," Opt. Lett. **16**, 986–988 (1991).
111. S. Trillo, G. Millot, E. Seve, and S. Wabnitz, "Failure of phase-matching concept in large-signal parametric frequency conversion," Appl. Phys. Lett. **72**, 150–152 (1998).
112. E. Seve, G. Millot, S. Trillo, and S. Wabnitz, "Large-signal enhanced frequency conversion in birefringent optical fibers: theory and experiments," J. Opt. Soc. Am. B **15**, 2537–2551 (1998).
113. G. Millot, E. Seve, S. Wabnitz, and S. Trillo, "Observation of a novel large-signal four-photon instability in optical wave mixing," Phys. Rev. Lett. **80**, 504–507 (1998).
114. C. De Angelis, M. Santagiustina, and S. Trillo, "Four-photon homoclinic instabilities in nonlinear highly birefringent media," Phys. Rev. A **51**, 774–791 (1995).
115. E. Seve, G. Millot, and S. Trillo, "Strong four-photon conversion regime of cross-phase-modulation-induced modulational instability," Phys. Rev. E **61**, 3139–3150 (2000).
116. R. J. Kruhlak, G. K. L. Wong, J. S. Y. Chen, S. G. Murdoch, R. Leonhardt, J. D. Harvey, N. Y. Joly, and J. C. Knight, "Polarization modulation instability in photonic crystal fibers," Opt. Lett. **31**, 1379–1381 (2006).
117. P. Russell, "Photonic crystal fibers," Science **299**, 358–362 (2003).
118. A. Hasegawa, "Generation of a train of soliton pulses by induced modulational instability in optical fibers," Opt. Lett. **9**, 288–290 (1984).
119. S. Trillo and S. Wabnitz, "Ultrashort pulse train generation through induced modulational polarization instability in a birefringent Kerr-like medium," J. Opt. Soc. Am. B **6**, 238–249 (1989).
120. G. Millot, E. Seve, S. Wabnitz, and M. Haelterman, "Dark-soliton-like pulse-train generation from induced modulational polarization instability in a birefringent fiber," Opt. Lett. **23**, 511–513 (1998).
121. Y. S. Kivshar and S. K. Turitsyn, "Vector dark solitons," Opt. Lett. **18**, 337–339 (1993).
122. E. Seve, G. Millot, and S. Wabnitz, "Buildup of terahertz vector dark-soliton trains from induced modulation instability in highly birefringent optical fiber," Opt. Lett. **23**, 1829–1831 (1998).
123. E. Seve, G. Millot, S. Wabnitz, T. Sylvestre, and H. Maillotte, "Generation of vector dark soliton trains by induced modulational instability in a highly birefringement fiber," J. Opt. Soc. Am. B **16**, 1642–1650 (1999).
124. J. M. Dudley, F. Gutty, S. Pitois, and G. Millot, "Complete characterization of THz pulse trains generated from nonlinear processes in optical fibers," IEEE J. Quantum Electron. **37**, 587–594 (2001).
125. G. Millot, P. Tchofo Dinda, E. Seve, and S. Wabnitz, "modulational instability and stimulated Raman scattering in normally dispersive highly birefringent fibers," Opt. Fiber Technol. **7**, 170–205 (2001).
126. Y. S. Kivshar, M. Haelterman, P. Emplit, and J. P. Hamaide, "Gordon–Haus effect on dark solitons," Opt. Lett. **19**, 19–21 (1994).
127. A. Tonello, S. Pitois, S. Wabnitz, G. Millot, T. Martynkien, W. Urbanczyk, J. Wojcik, A. Locatelli, M. Conforti, and C. De Angelis, "Frequency tunable polarization and intermodal modulation instability in high birefringence holey fiber," Opt. Express **14**, 397–404 (2006).
128. K. Tarnowski, A. Anuszkiewicz, J. Olszewski, P. Mergo, B. Kibler, and W. Urbanczyk, "Nonlinear frequency conversion in a birefringent microstructured fiber tuned by externally applied hydrostatic pressure," Opt. Lett. **38**, 5260–5263 (2013).
129. A. Kudlinski, A. Bendahmane, D. Labat, S. Virally, R. T. Murray, E. J. R. Kelleher, and A. Mussot, "Simultaneous scalar and cross-phase modulation instabilities in highly birefringent photonic crystal fiber," Opt. Express **21**, 8437–8443 (2013).
130. G. Millot, "Multiple four-wave mixing-induced modulational instability in highly birefringent fibers," Opt. Lett. **26**, 1391–1393 (2001).
131. J. Fatome, I. El-Mansouri, J.-L. Blanchet, S. Pitois, G. Millot, S. Trillo, and S. Wabnitz, "Even harmonic pulse train generation by cross-polarization-modulation seeded instability in optical fibers," J. Opt. Soc. Am. B **30**, 99–106 (2013).
132. A. Tonello, S. Wabnitz, T. Martynkien, G. Golojuch, and W. Urbanczyk, "Control of modulation and soliton polarization instabilities in photonic crystal fibers with birefringence management," Opt. Quantum Electron **39**, 435–453 (2007).